

Reduced order model for nonlinear multi-directional ocean wave propagation

Cite as: Phys. Fluids **33**, 117115 (2021); <https://doi.org/10.1063/5.0070246>

Submitted: 05 September 2021 • Accepted: 31 October 2021 • Published Online: 18 November 2021

 Sandeep Reddy Bukka, Yun Zhi Law, Harrif Santo, et al.



View Online



Export Citation



CrossMark

ARTICLES YOU MAY BE INTERESTED IN

[Numerical investigation of three-dimensional asymmetric hovering flapping flight](#)
Physics of Fluids **33**, 111907 (2021); <https://doi.org/10.1063/5.0069840>

[Modification of flow behind a circular cylinder by steady and time-periodic blowing](#)
Physics of Fluids **33**, 115126 (2021); <https://doi.org/10.1063/5.0067706>

[The electro-osmotic flow and heat transfer of generalized Maxwell fluids with distributed-order time-fractional characteristics in microtubules under an alternating field](#)
Physics of Fluids **33**, 113105 (2021); <https://doi.org/10.1063/5.0073752>

Physics of Fluids

SPECIAL TOPIC: Flow and Acoustics of Unmanned Vehicles

Submit Today!



Reduced order model for nonlinear multi-directional ocean wave propagation

Cite as: Phys. Fluids **33**, 117115 (2021); doi: [10.1063/5.0070246](https://doi.org/10.1063/5.0070246)

Submitted: 5 September 2021 · Accepted: 31 October 2021 ·

Published Online: 18 November 2021





View Online



Export Citation



CrossMark

Sandeep Reddy Bukka,^{1,2,a)}  Yun Zhi Law,^{2,b)} Harrif Santo,^{2,c)} and Eng Soon Chan^{2,3,d)} 

AFFILIATIONS

¹Max Planck Institute for Dynamics of Complex Technical Systems, Magdeburg 39106, Germany

²Technology Centre for Offshore and Marine, Singapore (TCOMS), Singapore 118411, Singapore

³Department of Civil and Environmental Engineering, National University of Singapore, Singapore 117576, Singapore

^{a)}Author to whom correspondence should be addressed: bukka@mpi-magdeburg.mpg.de

^{b)}Electronic mail: law_yun_zhi@tcoms.sg

^{c)}Electronic mail: harrif_santo@tcoms.sg

^{d)}Electronic mail: tcoces@tcoms.sg

ABSTRACT

In this paper, we introduce a reduced order model (ROM) for the propagation of nonlinear multi-directional ocean wave-fields. The ROM relies on Galerkin projection of Zakharov equations embedded in the high-order spectral (HOS) method, which describes the evolution of nonlinear waves. The dominant flow features of wave evolution are computed from proper orthogonal decomposition (POD) and these modes are used for the projection. The HOS scheme to compute the vertical velocity is treated in a novel way for an efficient implementation of POD-based ROM. We refer to this alternative formalism of HOS as HOS-simple. The final reduced order model (ROM) is derived from the Galerkin projection of HOS-simple. For the case of irregular waves, where the number of modes required are in the range of 200, the ROM has no significant advantage since both HOS and HOS-simple are much faster than real-time. The real advantage is demonstrated in multi-directional (or short-crested) irregular waves, where the ROM is the only model capable of achieving real-time computation, a major improvement to the standard HOS method. The potential use of the ROM in propagating short-crested waves from far-field to near-field for real-world applications involving wave probes in a wave tank/controlled environment as well as X-band radar in open ocean is also demonstrated.

© 2021 Author(s). All article content, except where otherwise noted, is licensed under a Creative Commons Attribution (CC BY) license (<http://creativecommons.org/licenses/by/4.0/>). <https://doi.org/10.1063/5.0070246>

I. INTRODUCTION

Fast and accurate prediction of ocean wave-fields is becoming increasingly important for marine and offshore industries. With the ongoing digitalization effort undertaken by industries to enhance the safety, productivity, and reliability of their systems and the associated operations, the ability to predict the operating environment, starting with ocean wave-fields, will contribute to the digitalization effort. This ability also helps to shape out future systems, such as navigation of autonomous vessels and the development of smart and intelligent off-shore and marine renewable energy systems.

In general, two types of wave prediction models exist: phase-averaged and phase-resolved models. Phase-averaged models are well-established and have existed for several decades.^{3,17,35} These models describe the evolution of wave spectra and produce wave spectra or statistics that describe significant wave heights, spectral periods, and wave propagation directions. Wave-by-wave prediction models that

are phase-resolving, on the other hand, are still in their infancy. For short-term predictions, say a few tens of seconds to minutes in the future, the actual ocean surface profile is predicted as a function of space and time.^{18,22,37} The general practice is to use phase-averaged models to study wave climate conditions, while the phase-resolved models are critical for scenarios that require precise knowledge of the sea surface elevation at a given time and location, such as autonomous navigation, marine operations, and development of real-time digital met-ocean.

Numerous nonlinear wave models have been created during the last few decades to solve the nonlinear evolution of sea-state over large domains for long time periods. The majority of them were created within the framework of potential flow theory, taking into account the fact that ocean wave propagation is essentially irrotational and inviscid (until the point of wave breaking or where strong wave-current interaction exists). Several attempts have been made to solve the whole

Euler or Navier–Stokes equations. However, due to the computational work required, the solution is limited to small domain scales. In parallel, solving the fully nonlinear potential flow formulation efficiently and accurately remains a significant challenge. For a comprehensive overview on various numerical approaches used for modeling the evolution of nonlinear ocean waves, the readers are referred to Ref. 13. This excellent review by Fenton contains salient features of the most important numerical models such as finite difference, finite element, boundary element, pseudo-spectral methods, Green–Naghdi theory, and local polynomial approximations in the context of nonlinear wave models.

Due to its pseudo-spectral formalism, the high-order spectral (HOS) method is highly efficient and accurate in this setting. When dealing with the propagation of open-ocean wave-fields at constant sea depth, it has been demonstrated that the HOS method is more efficient than advanced models that solve the volume problem using finite-difference discretization.⁸ Numerous authors have extensively employed and validated the HOS method to investigate a variety of physical mechanisms, including nonlinear energy transfers,³² modulational instabilities,^{14,33} bi-modal seas,³⁴ and freak waves.^{10,30,40} As a result, this method can be regarded as mature and applicable to real-world engineering problems. Despite all the advantages of the HOS method, it is still computationally expensive to solve the nonlinear evolution of multi-directional ocean wave-fields in real-time.^{22,28} The main objective of the present work is to overcome this limitation of the HOS method in terms of computational speed via reduced order modeling (ROM), while retaining its inherent advantages listed above.

Proper orthogonal decomposition (POD) is a mathematical approach for extracting a basis for a modal decomposition from an ensemble of signals. Kosambi,²³ Loève and Karhunen^{20,24} independently proposed the methodology, which is sometimes referred to as Kosambi–Karhunen–Loève theorem. However, comparable approaches have been developed across a range of diverse fields.³⁹ In statistics, the process is referred to as principal component analysis (PCA) whereas in oceanography and meteorology, it is referred to as the method of empirical orthogonal functions (EOFs).¹² POD has been effectively employed in a broad variety of domains, including signal analysis and pattern recognition,¹⁵ fluid dynamics and coherent structures,¹⁹ and image reconstruction.²¹

A significant innovation in the application of POD to big problems in fluid dynamics is the use of a series of snapshots, which is composed of a collection of state solutions evaluated at various time instants and calculated from the model's temporal evolution. The snapshots are used to compute the POD basis vectors in order to obtain an optimal representation of the data such that the two-norm of the error between the original and reconstructed snapshots is minimized for any given basis vector size. Additionally, it has been demonstrated that POD technique combined with the Galerkin projection procedure is an efficient method for creating reduced order models.²⁵ This technique derives the most energetic modes in a time-dependent system, allowing for the construction of a low-dimensional description of the system's dynamics. The field of reduced order modeling is vast, and novel techniques are being developed at a rapid rate. The readers are referred to Refs. 1 and 29 for a review on projection-based model reduction techniques and to Refs. 4 and 31 for a complete survey of model reduction for turbulence control methods and modal analysis of fluid flows.

The Galerkin projection falls under intrusive methods for model order reduction. Recently with the introduction of machine learning to fluid mechanics, there have been numerous attempts to develop nonintrusive models for model order reduction.^{5,11,27} In particular, the work by Maulik *et al.*²⁶ developed a nonintrusive model via deep auto-encoders for shallow water equations. The focus of this article is on intrusive model order reduction for the evolution of ocean waves. For the first time, this work attempts to develop a projection-based reduced order model of the HOS method to solve for the nonlinear evolution of ocean wave-fields. Galerkin projection of nonlinear free surface boundary conditions is carried out to obtain a low-dimensional model. The projection is carried out on the POD modes obtained from the snapshot data. The main motivation behind this work is to develop a real-time model that can describe the nonlinear evolution of multi-directional waves or short-crested seas.

The article is organized as follows. Section II gives a brief description of the high-dimensional model. Section III describes the detailed mathematical formulations and the development of projection-based reduced order models. Section IV presents the results from the numerical experiments on unidirectional and multi-directional irregular waves. Section V discusses their potential use for real-world applications, and Sec. VI concludes the present study.

II. HIGH-DIMENSIONAL MODEL

The formulation behind the HOS methods of Refs. 7 and 36 is presented in this section briefly. The flow is considered to be irrotational, homogenous, incompressible, and inviscid under a free surface. The governing equations for the HOS method are formulated in terms of surface velocity potential ψ and wave elevation η . They are obtained from the kinematic and dynamic free surface boundary condition of free surface flow, written as follows:

$$\begin{aligned} \frac{\partial \psi}{\partial t} + g\eta + 0.5 * \left(\frac{\partial \psi}{\partial x} \right)^2 - 0.5 \left(\frac{\partial \tau}{\partial z} \Big|_{z=\eta} \right)^2 \left\{ 1 + \left(\frac{\partial \eta}{\partial x} \right)^2 \right\} &= 0, \\ \frac{\partial \eta}{\partial t} + \frac{\partial \psi}{\partial x} * \frac{\partial \eta}{\partial x} - \left(\frac{\partial \tau}{\partial z} \Big|_{z=\eta} \right) \left\{ 1 + \left(\frac{\partial \eta}{\partial x} \right)^2 \right\} &= 0. \end{aligned} \quad (1)$$

The premise of the HOS scheme is in the expansion derived for the term $\frac{\partial \tau}{\partial z} \Big|_{z=\eta}$ given as

$$\begin{aligned} \frac{\partial \tau}{\partial z} &= \sum_{m=1}^M \sum_{i=0}^{m-1} \eta^i \frac{\partial^{i+1}}{\partial z^{i+1}} \tau^{m-i}, \\ \tau^m &= - \sum_{i=1}^{m-1} \frac{\eta^i}{i!} \frac{\partial^i}{\partial z^i} \tau^{m-i}, \\ \tau^1 &= \psi. \end{aligned} \quad (2)$$

The detailed numerical procedure to solve Eqs. (1) and (2) is given in Ref. 16 and readers are referred to the same for further details. In this study, the open-source code HOS-Ocean code developed by Ecole Centrale de Nantes (ECN) is used, see Refs. 2 and 9. The formulation behind the evolution engine HOS-Ocean is not the main target of this paper and therefore only the necessary details are presented here for the sake of brevity. HOS-Ocean is used to generate synthetic nonlinear wave-fields.

III. REDUCED ORDER MODEL

The basic theory behind model order reduction and POD is outlined first in this section. Consider a general nonlinear governing equation consisting of linear and nonlinear parts written as follows:

$$\mathbf{L}\mathbf{x} + \mathbf{f}(\mathbf{x}) = \mathbf{0}, \quad (3)$$

where $\mathbf{L} \in \mathbb{R}^{N \times N}$ denotes the linear part of the governing equation and $\mathbf{f} \in \mathbb{R}^{N \times N}$ embeds the nonlinear part, and $\mathbf{x} \in \mathbb{R}^N$ denotes the state of the system at hand. The basic principle of model order reduction is to represent \mathbf{x} using a reduced basis $\Phi \in \mathbb{R}^{N \times r}$ and corresponding modal coefficient $\alpha_x \in \mathbb{R}^r$, where

$$\mathbf{x} = \Phi \alpha_x. \quad (4)$$

The reduced basis Φ can be computed using POD. Let $\mathcal{X} = \{\mathbf{x}_1, \mathbf{x}_2, \dots, \mathbf{x}_{nt}\}$ be the snapshot matrix containing the solutions of the state for a finite number, nt , of time steps. The POD procedure involves computing a singular value decomposition (SVD) on this snapshot matrix to obtain the reduced basis Φ .

Substituting \mathbf{x} from Eq. (4) into Eq. (3) and taking the orthogonal projection of the equation onto the reduced basis, we get

$$\begin{aligned} \Phi^T \mathbf{L} \Phi \alpha_x + \Phi^T \mathbf{f}(\Phi \alpha_x) &= \mathbf{0}, \\ \tilde{\mathbf{L}} \alpha_x + \Phi^T \mathbf{f}(\Phi \alpha_x) &= \mathbf{0}. \end{aligned} \quad (5)$$

It can be observed that by taking the orthogonal projection, we are effectively reducing the dimension of the problem from N to m . However, the nonlinear term $\Phi^T \mathbf{f}(\Phi \alpha_x) = \mathbf{0}$ still has computational operations to be performed in the order of N computation to be performed. To alleviate this difficulty, the Discrete Element Interpolation Method (DEIM) method proposed by Ref. 6, which approximates the nonlinear function at few sampling points $m \ll N$ and interpolates at all other locations. DEIM also uses POD on the set of nonlinear snapshots $\mathcal{F} = \{\mathbf{f}_1, \mathbf{f}_2, \dots, \mathbf{f}_{nt}\}$ to compute the reduced basis $\Phi_f \in \mathbb{R}^{N \times r}$ for the nonlinear function \mathbf{f} . The interpolation matrix $\mathbf{P} = [e_1, e_2, \dots, e_m] \in \mathbb{R}^{N \times r}$ where $e_i \in \{0, 1\}^N$ is constructed using QR decomposition of the nonlinear reduced basis Φ_f . The DEIM approximation of the nonlinear function \mathbf{f} is given by

$$\mathbf{f}(\mathbf{x}) = \Phi_f (\mathbf{P}' \Phi_f)^{-1} \mathbf{P}' \mathbf{f}(\mathbf{x}). \quad (6)$$

The key term in the above equation is $\mathbf{P}' \mathbf{f}(\mathbf{x})$, which is the nonlinear function sampled at m points and has the order of m computation. The DEIM interpolant $\Phi_f (\mathbf{P}' \Phi_f)^{-1}$ can be pre-computed before the start of the real-time computation and therefore reduces the order of computation from N to m . The reduced system of equations to be solved is given as follows:

$$\tilde{\mathbf{L}} \alpha_x + \Phi^T \Phi_f (\mathbf{P}' \Phi_f)^{-1} \mathbf{P}' \mathbf{f}(\Phi \alpha_x) = \mathbf{0}. \quad (7)$$

Applying this to the governing equations of the HOS method [Eq. (1)], we first re-write in a simpler format by grouping them between linear and nonlinear terms, expressed as follows:

$$\begin{aligned} \frac{\partial \psi}{\partial t} + g\eta + \psi_{NL} &= 0, \\ \frac{\partial \eta}{\partial t} - \left(\frac{\partial \tau^1}{\partial z} \right) + \eta_{NL} &= 0, \end{aligned} \quad (8)$$

where $\tau^1 = \psi$ from the HOS scheme. Substituting $\eta = \phi_\eta \alpha_\eta$ and $\psi = \phi_\psi \alpha_\psi$ and taking orthogonal projection with ϕ_η, ϕ_ψ on the above equation, we obtain

$$\begin{aligned} \frac{\partial \alpha_\psi}{\partial t} + \phi'_\psi g \phi_\eta \alpha_\eta + \phi'_\psi \psi_{NL} &= 0, \\ \frac{\partial \alpha_\eta}{\partial t} - \phi'_\eta \frac{\partial \phi_\psi}{\partial z} \alpha_\psi + \phi'_\eta \eta_{NL} &= 0. \end{aligned} \quad (9)$$

The interpolation matrices P_η, P_ψ are computed for nonlinear terms η_{NL} and ψ_{NL} and DEIM approximation is used in the above equation to obtain the reduced system of equations, written as follows:

$$\begin{aligned} \frac{\partial \alpha_\psi}{\partial t} + \left(\phi'_\psi g \phi_\eta \right) \times \alpha_\eta + \phi'_\psi \phi_{\psi_{NL}} \left\{ P'_\psi \phi_{\psi_{NL}} \right\}^{-1} \psi_{NL}^P, \\ \frac{\partial \alpha_\eta}{\partial t} - \left(\phi'_\eta \frac{\partial \phi_\psi}{\partial z} \right) \times \alpha_\psi + \phi'_\eta \phi_{\eta_{NL}} \left\{ P'_\eta \phi_{\eta_{NL}} \right\}^{-1} \eta_{NL}^P, \end{aligned} \quad (10)$$

where η_{NL}^P and ψ_{NL}^P are nonlinear terms computed at discrete sampling points. Before proceeding to formulation details of η_{NL}^P and ψ_{NL}^P , we must first address the computation of $\frac{\partial \tau}{\partial z}$ and its reduced order form.

From the HOS scheme, $\frac{\partial \tau}{\partial z}$ is given in Eq. (2) where $\tau^1 = \psi$. Substituting the modal decomposition of η and ψ into Eq. (2) and rearranging the spatial and temporal components together, we derive the reduced form of the operator $\frac{\partial \tau}{\partial z}$ as

$$\begin{aligned} \left(\frac{\partial \tau}{\partial z} \right)_{r1} &= \sum_{m=1}^M \sum_{i=0}^{m-1} \frac{1}{i!} \left[\phi_\eta^{i\otimes} \otimes \frac{\partial^{i+1}}{\partial z^{i+1}} \phi_\tau^{(m-i)} \right] * \left[\alpha_\eta^{i\otimes} \otimes \alpha_\tau^{(m-i)} \right], \\ \phi_\tau^{(m)} &= \sum_{i=1}^{M-1} \phi_\eta^{i\otimes} \otimes \frac{\partial^i}{\partial z^i} \phi_\tau^{(m-i)}, \\ \alpha_\tau^{(m)} &= \alpha_\eta \otimes \alpha_\tau^{(m-1)}, \\ \alpha_\tau^{(1)} &= \alpha_\psi, \quad \phi_\tau^{(1)} = \phi_\psi, \end{aligned} \quad (11)$$

where the notation $(\cdot)_{r1}$ denotes the first reduced order formulation for the operator $\frac{\partial \tau}{\partial z}$. A second reduced order formulation for the same operator is also presented in later parts of this section. The definition of the operator \otimes is given as

$$\begin{aligned} \alpha &= [\alpha_1, \alpha_2], \quad \beta = [\beta_1, \beta_2], \\ \alpha^{2\otimes} &= [\alpha_1^2, \alpha_1 \alpha_2, \alpha_2 \alpha_1, \alpha_2^2], \\ \alpha \otimes \beta &= [\alpha_1 \beta_1, \alpha_1 \beta_2, \alpha_2 \beta_1, \alpha_2 \beta_2]. \end{aligned} \quad (12)$$

The spatial derivatives $\frac{\partial(\eta, \psi)}{\partial(x, z)}$ present in the nonlinear terms are computed by taking spectral derivatives of the respective spatial modes (ϕ_η, ϕ_ψ) as follows:

$$\begin{aligned} \frac{\partial \eta}{\partial x} &= \frac{\partial \phi_\eta}{\partial x} \alpha_\eta, \quad \frac{\partial \psi}{\partial x} = \frac{\partial \phi_\psi}{\partial x} \alpha_\psi, \\ \frac{\partial \eta}{\partial z} &= \frac{\partial \phi_\eta}{\partial z} \alpha_\eta, \quad \frac{\partial \psi}{\partial z} = \frac{\partial \phi_\psi}{\partial z} \alpha_\psi, \\ \frac{\partial(\cdot)}{\partial x} &= \text{ifft}(\text{fft}(\cdot)) * 1i * \mathbf{k}, \quad \frac{\partial(\cdot)}{\partial z} = \text{ifft}(\text{fft}(\cdot)) * \mathbf{k} \tan h(\mathbf{k} * h). \end{aligned} \quad (13)$$

With the above formulations, the nonlinear terms η_{NL}^P and ψ_{NL}^P are computed as follows:

$$\begin{aligned}\psi_{NL}^P &= 0.5 \left(P_\psi \frac{\partial \phi_\psi}{\partial x} \alpha_\psi \right)^2 - 0.5 \left(P_\psi \left(\frac{\partial \tau}{\partial z} \right)_{r1} \right)^2 \left\{ 1 + \left(P_\psi \frac{\partial \phi_\eta}{\partial x} \alpha_\eta \right)^2 \right\}, \\ \eta_{NL}^P &= \left(P_\eta \frac{\partial \phi_\psi}{\partial z} \alpha_\psi \right) + \left(P_\eta \frac{\partial \phi_\psi}{\partial x} \alpha_\psi \right) * \left(P_\eta \frac{\partial \phi_\eta}{\partial x} \alpha_\eta \right) \\ &\quad - \left(P_\eta \left(\frac{\partial \tau}{\partial z} \right)_{r1} \right) \left\{ 1 + \left(P_\eta \frac{\partial \phi_\eta}{\partial x} \alpha_\eta \right)^2 \right\}.\end{aligned}\quad (14)$$

The final reduced order model of the HOS equations is given as follows:

$$\begin{aligned}\frac{\partial \alpha_\psi}{\partial t} &= - \left(\phi'_\psi g \phi_\eta \right) \times \alpha_\eta - \phi'_\psi \phi_{\psi NL} \left\{ P'_\psi \phi_{\psi NL} \right\}^{-1} \psi_{NL}^P, \\ \frac{\partial \alpha_\eta}{\partial t} &= \left(\phi'_\eta \frac{\partial \phi_\psi}{\partial z} \right) \times \alpha_\psi - \phi'_\eta \phi_{\eta NL} \left\{ P'_\eta \phi_{\eta NL} \right\}^{-1} \eta_{NL}^P, \\ \psi_{NL}^P &= 0.5 \left(P_\psi \frac{\partial \phi_\psi}{\partial x} \alpha_\psi \right)^2 - 0.5 \left(P_\psi \left(\frac{\partial \tau}{\partial z} \right)_{r1} \right)^2 \\ &\quad \times \left\{ 1 + \left(P_\psi \frac{\partial \phi_\eta}{\partial x} \alpha_\eta \right)^2 \right\}, \\ \eta_{NL}^P &= \left(P_\eta \frac{\partial \phi_\psi}{\partial z} \alpha_\psi \right) + \left(P_\eta \frac{\partial \phi_\psi}{\partial x} \alpha_\psi \right) * \left(P_\eta \frac{\partial \phi_\eta}{\partial x} \alpha_\eta \right) \\ &\quad - \left(P_\eta \left(\frac{\partial \tau}{\partial z} \right)_{r1} \right) \left\{ 1 + \left(P_\eta \frac{\partial \phi_\eta}{\partial x} \alpha_\eta \right)^2 \right\}, \\ \left(\frac{\partial \tau}{\partial z} \right)_{r1} &= \sum_{m=1}^M \sum_{i=0}^{m-1} \frac{1}{i!} \left[\phi_\eta^{i\otimes} \otimes \frac{\partial^{i+1}}{\partial z^{i+1}} \phi_\tau^{(m-i)} \right] * \left[\alpha_\eta^{i\otimes} \otimes \alpha_\tau^{(m-i)} \right], \\ \phi_\tau^{(m)} &= \sum_{i=1}^{M-1} \phi_\eta^{i\otimes} \otimes \frac{\partial^i}{\partial z^i} \phi_\tau^{(m-i)}, \\ \alpha_\tau^{(m)} &= \alpha_\eta \otimes \alpha_\tau^{(m-1)}, \\ \alpha_\tau^{(1)} &= \alpha_\psi, \quad \phi_\tau^{(1)} = \phi_\psi.\end{aligned}\quad (15)$$

The order of the HOS equations N is reduced to r in the above reduced order model. However, it can be observed from the term $\left(\frac{\partial \tau}{\partial z} \right)_{r1}$ that the order of computation is of $O(r^m)$ where m is the non-linear order of the HOS scheme. The exponential nature of this computation cannot be avoided and can be inefficient for a finite quantity of r and m . From our numerical experiments, we find that the computational cost of the above reduced order model with $r = 6$, $M = 5$ will be similar to that of standard HOS scheme with $N = 1024$, $M = 5$. The computational complexity of standard HOS scheme is $O(NM \log N)$. With the current formulation of $\left(\frac{\partial \tau}{\partial z} \right)_{r1}$, the reduced order model does not provide any significant gain in the computational speed for more realistic cases of unidirectional and multi-directional irregular waves where r tends to be around 50–100.

An alternative reduced order model for the operator $\frac{\partial \tau}{\partial z}$ is proposed in this work, which has the computational order of $O(r)$. The caveat to this alternative formulation is that it involves an approximation to the HOS scheme. From our numerical experiments, we find that this alternative formulation is applicable for waves with steepness $\frac{H_s}{T_p^2} \leq 0.1$ but has a phase difference with the results from the standard HOS scheme.

A. Alternative formulation for computation of $\frac{\partial \tau}{\partial z}$

In this section, we outline the alternative formulation for the computation of $\frac{\partial \tau}{\partial z}$ to alleviate the difficulties associated with computational complexity.

First, we modify the definition of wave elevation η . In the standard HOS formulation, the surface wave elevation is given by

$$\eta = \sum_j C_\eta(t) e^{i \mathbf{k}_j \cdot \vec{x}}. \quad (16)$$

We change the above definition of wave elevation by including a shape function dependent on z , written as

$$\eta = \sum_j C_\eta(t) \frac{\cosh(\mathbf{k}_j(z+d))}{\cosh(\mathbf{k}_j(d))} e^{i \mathbf{k}_j \cdot \vec{x}}, \quad z = \{0\}. \quad (17)$$

This shape function is introduced so that at $z=0$, η remains the same but $\frac{\partial \eta}{\partial z}$ exists. The direct manifestation of the above definition is the presence of $\frac{\partial \eta}{\partial z}$, which is used in the efficient simplification of the standard HOS scheme. First, we outline the details of the HOS scheme for $M=3$, written as follows:

$$\begin{aligned}\tau^1 &= \psi, & W^1 &= \frac{\partial \tau^1}{\partial z}, \\ \tau^2 &= -\eta \frac{\partial \tau^1}{\partial z}, & W^2 &= \frac{\partial \tau^2}{\partial z} + \eta \frac{\partial^2 \tau^1}{\partial z^2}, \\ \tau^3 &= -\eta \frac{\partial \tau^2}{\partial z} - \frac{\eta^2}{2!} \frac{\partial^2 \tau^1}{\partial z^2}, & W^3 &= \frac{\partial \tau^3}{\partial z} + \eta \frac{\partial^2 \tau^2}{\partial z^2} + \frac{\eta^2}{2!} \frac{\partial^3 \tau^1}{\partial z^3}, \\ & & \frac{\partial \tau}{\partial z} &= W^{(1)} + W^{(2)} + W^{(3)}.\end{aligned}$$

Now, with knowledge of the new formulation for η and the fact that $\frac{\partial \eta}{\partial z}$ exists, we derive the simplified HOS scheme as follows:

$$\begin{aligned}\tau^1 &= \psi, & W^1 &= \frac{\partial \tau^1}{\partial z}, \\ \tau^2 &= -\eta \frac{\partial \tau^1}{\partial z}, & W^2 &= \frac{\partial}{\partial z} \left(-\eta \frac{\partial \tau^1}{\partial z} \right) + \eta \frac{\partial^2 \tau^1}{\partial z^2}, \\ & & W^2 &= -\frac{\partial \eta}{\partial z} \frac{\partial \tau^1}{\partial z}, \\ \tau^3 &= -\eta \frac{\partial \tau^2}{\partial z} - \frac{\eta^2}{2!} \frac{\partial^2 \tau^1}{\partial z^2}, & W^3 &= \frac{\partial}{\partial z} \left(-\eta \frac{\partial}{\partial z} \left(-\eta \frac{\partial \tau^1}{\partial z} \right) - \frac{\eta^2}{2!} \frac{\partial^2 \tau^1}{\partial z^2} \right) \\ & & & + \eta \frac{\partial^2}{\partial z^2} \left(-\eta \frac{\partial \tau^1}{\partial z} \right) + \frac{\eta^2}{2!} \frac{\partial^3 \tau^1}{\partial z^3}, \\ & & W^3 &= \left(\frac{\partial \eta}{\partial z} \right)^2 \frac{\partial \tau^1}{\partial z}, \\ & & & \vdots \\ & & W^i &= -1^{i+1} \left(\frac{\partial \eta}{\partial z} \right)^{i-1} \frac{\partial \tau^1}{\partial z}, \\ \frac{\partial \tau}{\partial z} &= \sum_i W^i = \frac{\partial \tau^1}{\partial z} \left[1 - \left(\frac{\partial \eta}{\partial z} \right) + \left(\frac{\partial \eta}{\partial z} \right)^2 + \dots \right], \\ & & \frac{\partial \tau}{\partial z} &= \frac{\partial \tau^1}{\partial z} \frac{1}{1 + \frac{\partial \eta}{\partial z}}.\end{aligned}\quad (18)$$

Figure 1 compares the results from HOS, HOS-simple, and linear wave theory for $\frac{\partial \tau}{\partial z}$. By linear wave theory, we mean $\frac{\partial \tau}{\partial z} = \frac{\partial \tau^1}{\partial z}$. It can be seen that results from HOS-simple are closer to those from HOS than those from the linear wave theory, and both HOS-simple and HOS completely coincide as time progresses. We have also plotted $\frac{\partial \eta}{\partial z}$ in Fig. 2, which is the main difference between HOS-simple and linear theory. One can notice that the term $\frac{\partial \eta}{\partial z}$ has significant contribution and also possesses the nonlinear asymmetry between the crest and trough common to steeper waves.

Using the above alternative formulation, we define a second reduced order form for the operator $\frac{\partial \tau}{\partial z}$, which is given as follows:

$$\left(\frac{\partial \tau}{\partial z}\right)_{r2} = \frac{\frac{\partial \phi_\psi}{\partial z} \alpha_\psi}{1 + \frac{\partial \phi_\eta}{\partial z} \alpha_\eta}. \quad (19)$$

The order of computation in the above formulation is not of exponential nature but is linear on the order of $O(r)$. The reduced order model with $(\frac{\partial \tau}{\partial z})_{r1}$ is referred to as ROM1 and the one with $(\frac{\partial \tau}{\partial z})_{r2}$ is referred to as ROM2. The final equations for ROM2 are the same as for ROM1 [Eq. (15)], except for the term $(\frac{\partial \tau}{\partial z})_{r2}$.

Finally, the construction of ROM entails two major steps, which are as follows:

- computation of modes ϕ_ψ and ϕ_η from simulation data and
- computation of all the reduced operators in Eq. (15) before setting up the prediction of ROM. By reduced operators, we mean all the terms involving $\phi_{\eta,\psi}$.

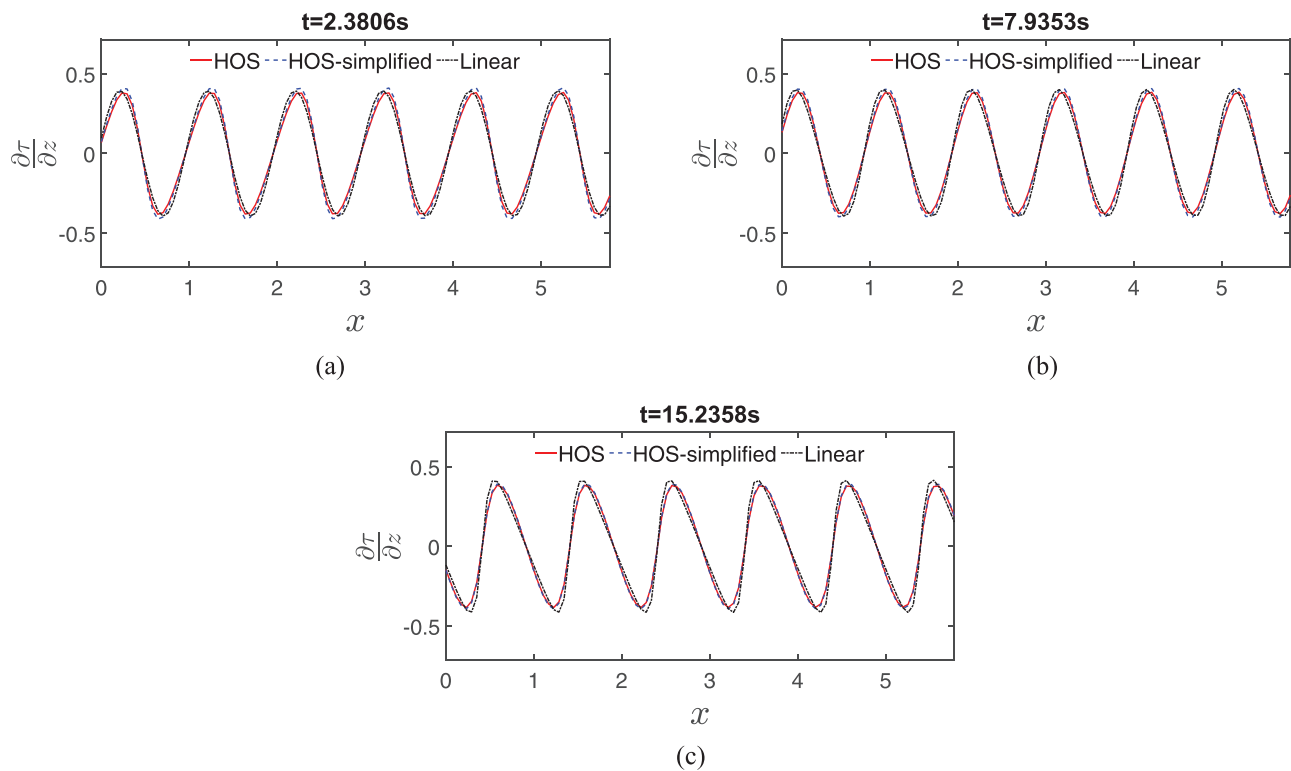


FIG. 1. Comparison of $\frac{\partial \tau}{\partial z}$ computed using the normal HOS scheme, HOS-simplified scheme, and linear version for regular wave case H0.1.

More comparisons between these two formulations are outlined in the Sec. III B in the context of regular waves.

B. Comparison of ROM formulations

In this section, we compare the results from ROM formulations, HOS, and HOS-simple presented in Sec. III A for three regular waves capturing different steepness characteristics.

Table I refers to the details of the cases considered for this analysis. For each case, simulations are carried out using the normal HOS scheme, simplified HOS scheme, ROM1, and ROM2. All the codes are written in MATLAB for the sake of consistency and for the development of ROMs. Common simulation parameters for the HOS method are presented in Table II.

As mentioned in Sec. III A, before proceeding for ROM simulations, one has to construct the ROM by computing the modes from POD of the simulation data and evaluating the reduced operators of the ROM equations. The number of ROM modes are chosen by examining the eigenvalues from the singular value decomposition (SVD).

Figure 3 depicts the cumulative energy of the POD modes, and Fig. 4 shows the effect of the number of POD modes and DEIM control points on the accuracy of the results, all for the case of regular wave H0.1. The midpoint (7, 20) is chosen for POD modes and DEIM points respectively for the case H0.1. Table III outlines the number of POD modes and DEIM points considered for all the three cases of regular waves. Upon choosing the number of modes, all the reduced operators of the system are pre-computed once before the start of ROM predictions. It should be noted that although one could have

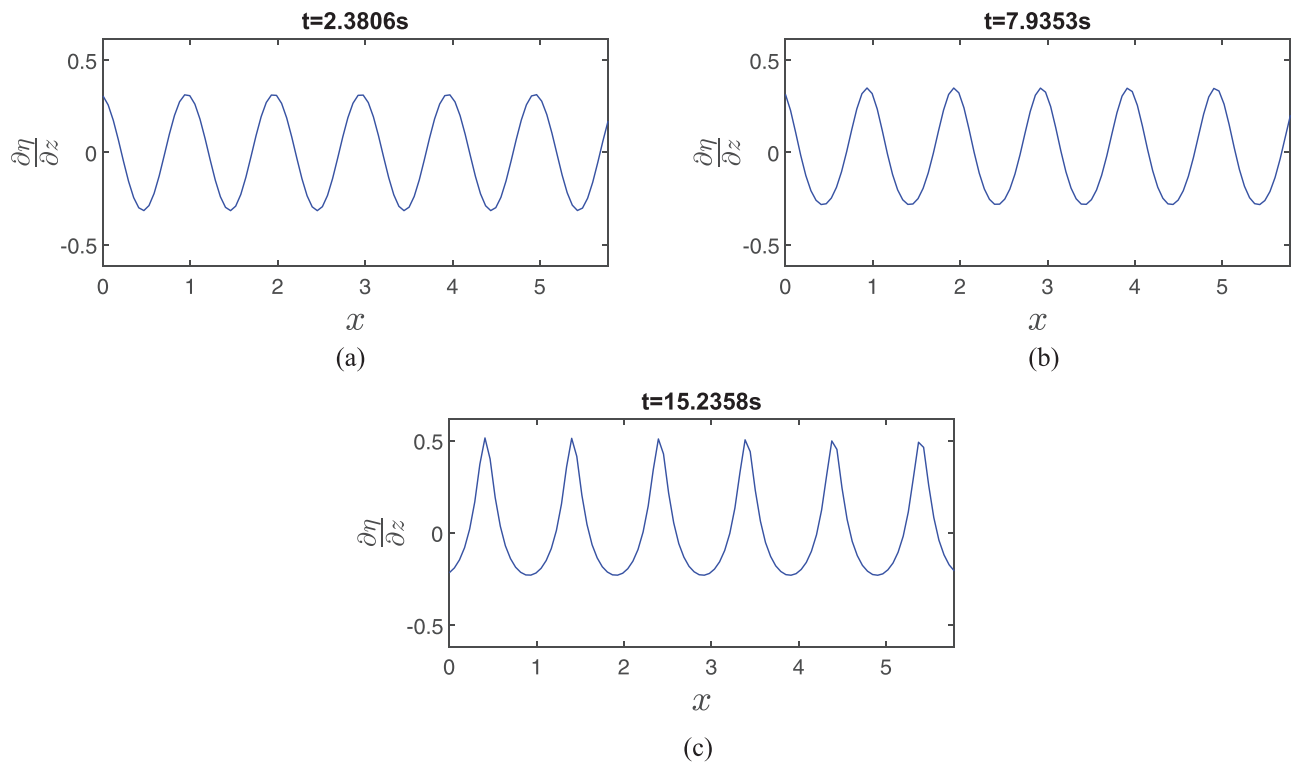


FIG. 2. Snapshots of $\frac{\partial \eta}{\partial z}$ at different time instants for regular wave case H0.1.

TABLE I. Regular wave cases considered for the analysis.

	H0.1	H0.05	H0.01
Water depth (m)	1	1	1
Wave length, λ (m)	1	1	1
Wave period, T (s)	0.761 79	0.790 49	0.799 91
Wave height, H (m)	0.1	0.05	0.01
Wave steepness, H/λ	10%	5%	1%

TABLE II. Common input simulation parameters for the HOS method: regular waves.

Parameter	Value
Frequency	$48/T$
Domain length	$60^* \lambda$
Discretization	1024
Relaxation period	$4^* T$
Nonlinear order	5

developed a single ROM for all the three cases considered here, we chose to build ROM separately for all the three cases for a qualitative comparison with the full order model results respectively.

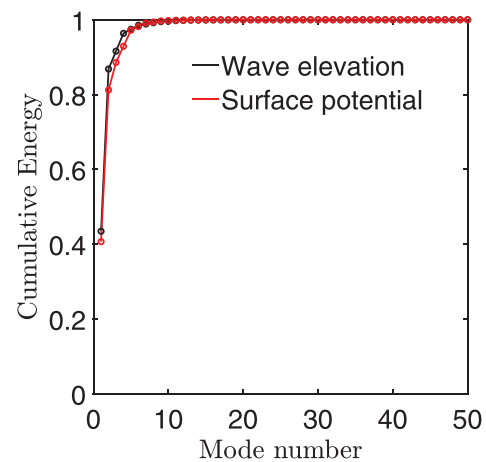


FIG. 3. Cumulative energy of POD modes of wave elevation and surface potential for regular wave H0.1.

The performance of the HOS-simple scheme is first assessed for all the regular wave cases and compared with the results from standard HOS scheme. Figure 5 provides the comparison. The HOS-simple scheme performs well for all three wave steepness values without getting destabilized. The nonlinear nature of steep waves, i.e., sharper and narrower crests compared to flatter troughs, is perfectly captured by

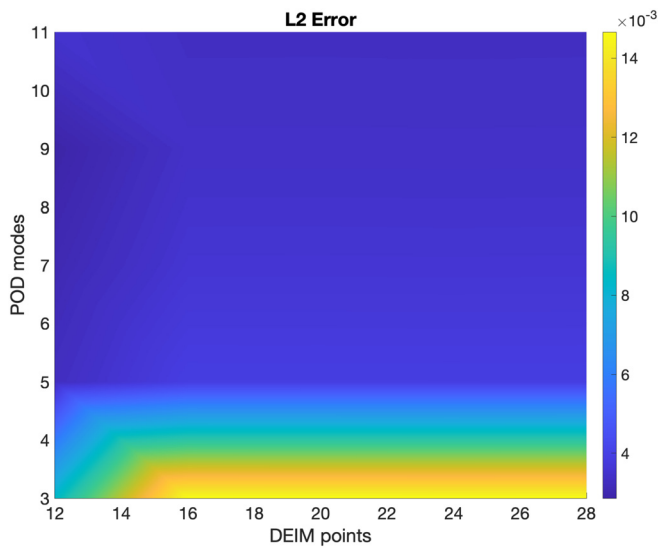


FIG. 4. Effect of the number of POD modes and DEIM points on the L2 error for regular wave H0.1.

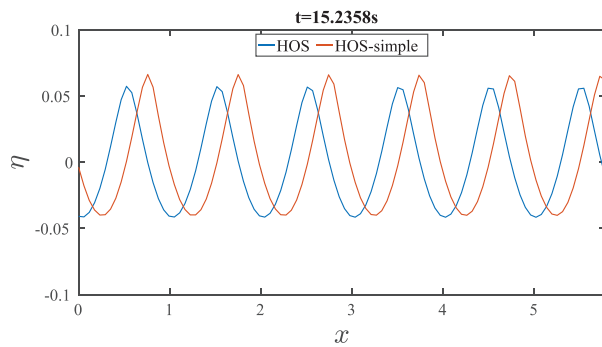
TABLE III. Number of POD and DEIM points considered for regular wave cases.

Case	POD modes	DEIM points
H0.01	3	8
H0.05	5	15
H0.1	7	20

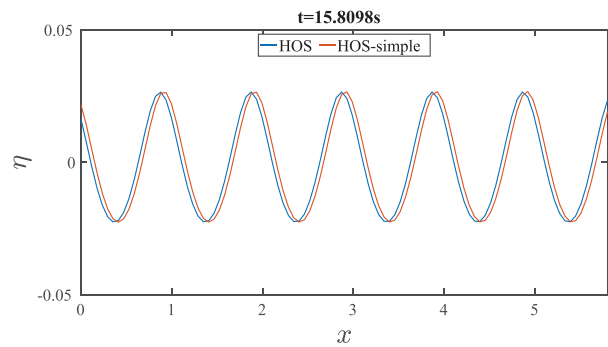
the HOS-simple scheme. However, there is a noticeable phase difference for the case of higher steepness H0.1. The phase difference is attributed to the approximations invoked in the derivation of the HOS-simple scheme. Further studies are being carried out to determine the cause and to minimize the difference.

Figure 6 presents a qualitative comparison of wave elevation obtained from HOS, ROM1, and ROM2. In terms of accuracy, ROM1 is much closer to the HOS results across all the cases whereas ROM2 deviates from HOS for the case of higher steepness (H0.1), which is expected since HOS-simple also deviates in a similar fashion. This deviation is in terms of phase difference of the solution and it should be noted that the nonlinearities associated with high steep waves are perfectly captured by ROM2.

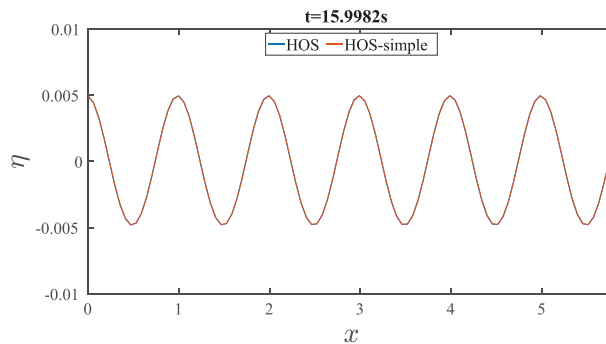
Quantitative comparisons of the computational speed between all the models (HOS, HOS-simple, ROM1, and ROM2) are provided



(a)



(b)



(c)

FIG. 5. Comparison of wave elevation between the HOS-simple and HOS schemes: (a) H0.1, (b) H0.05, and (c) H0.01.

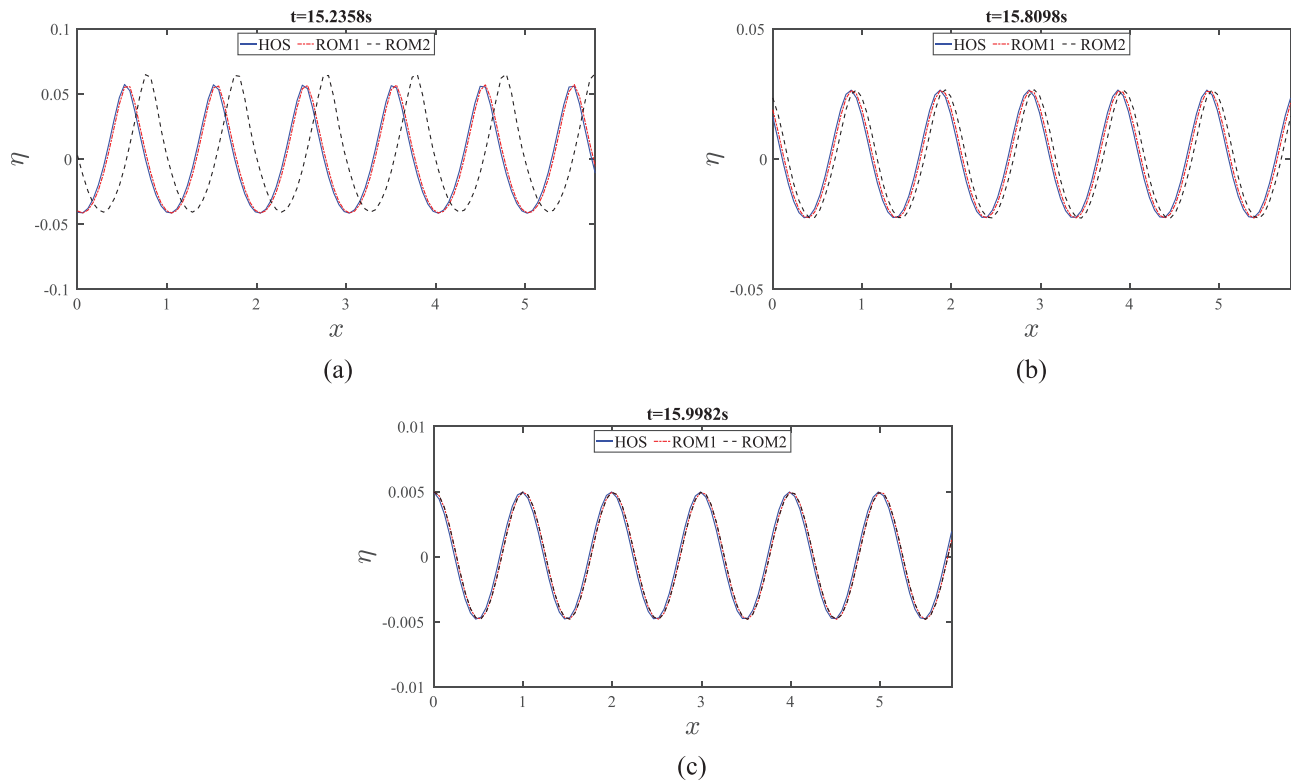


FIG. 6. Comparison of wave elevation between HOS and ROM: (a) $H_{0.1}$, (b) $H_{0.05}$, and (c) $H_{0.01}$.

in Fig. 7. The computational speed of the HOS-simple scheme is much faster than the standard HOS scheme. It can be seen that ROM2 is much faster by an order of magnitude compared to HOS-simple and two orders of magnitude compared to the standard HOS model.

ROM1 performs quite well for $M=3$ but loses its computational advantage for $M=5$. Therefore, solely based on their computational efficiency, ROM2 can be potentially used for practical applications requiring a phase-resolved forecast of the wave environment in

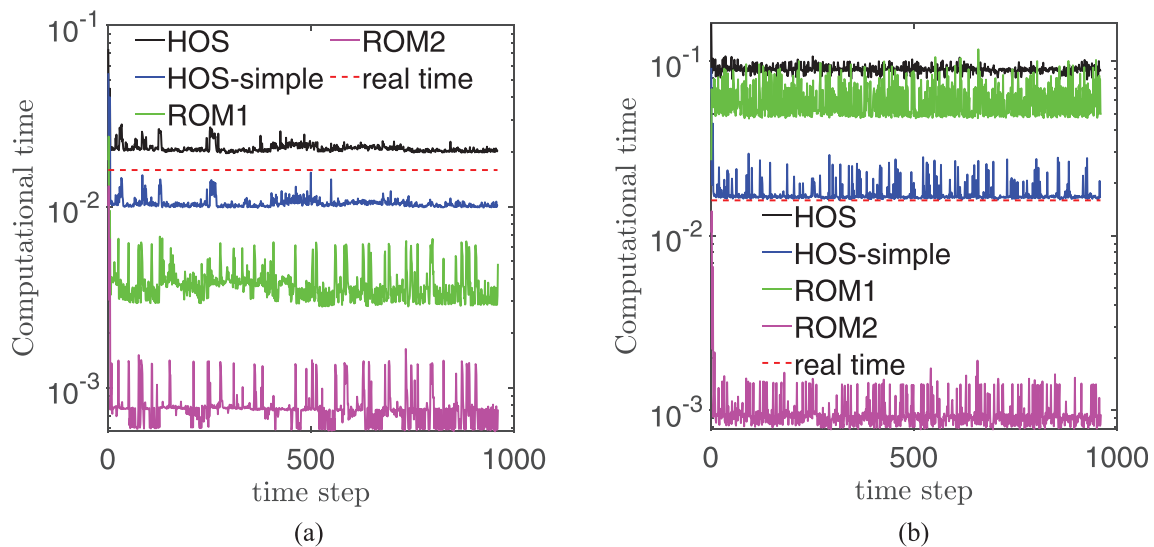


FIG. 7. Computational time comparison (a) $r=6, M=3$ and (b) $r=6, M=5$.

real-time. For the rest of this paper, the proposed reduced order model (ROM) is referred to as ROM2 in the plots.

IV. RESULTS

ROM2 is subsequently built based on training data from a general database. Subsequently, the performance of ROM2 is further investigated on completely unknown or unseen wave conditions. The analysis is carried out for unidirectional and multi-directional waves and is presented in Secs. IV A and IV B.

A. Unidirectional irregular waves

For the unidirectional irregular waves, we develop a general database of different wave conditions made up of six distinct sea-state steepness values and around 200 random wave realizations for each steepness. In total, 1200 wave simulations are carried out using HOS-Ocean⁹ to generate a synthetic database. We consider the range of steepness $0.01 - 0.06$ and waves with spectral peak period T_p ranging from 1.0 to 4.0 s. Note the scale used in the database is for a typical wave tank or basin but the methodology can be equally applied to the full-scale parameters encountered in open ocean.

The parameters of the irregular waves and solver settings for generating the synthetic database are depicted in Table IV. The operators of the reduced order model are computed from around 600 cases of training data and the prediction is carried out on completely unseen test cases with different steepness values and different wave conditions. Each wave simulation case has 3000 snapshots; however, we only consider every tenth snapshot for basis generation to reduce the data to be handled and also to consider sufficient distinctions between adjacent snapshots.

Figure 8 shows the cumulative energy captured by the POD modes in the system. Around 200 POD modes and 300 DEIM control points are used to construct the reduced order operators in the offline computation phase. ROM2 is also integrated in time with the same time step $dt = 0.1$ s to generate the results. Figure 9 depicts the computational time required by HOS, HOS-simple, and ROM2 for a single case for qualitative comparison. All the schemes perform faster than real-time. ROM2 with $r = 200$ is slower than its full order counterpart, HOS-simple, but a bit faster than the standard HOS model. The computational cost of ROM2 exceeds that of HOS-simple in this case,

TABLE IV. Parameters used to generate synthetic database of unidirectional irregular waves.

	Train			Test		
Sea-state steepness (H_s/T_p^2)	0.02	0.04	0.06	0.01	0.03	0.05
T_p (s)	1.0–4.0					
H_s (m)	Steepness* T_p^2					
Cases	200 Each					
Common simulation parameters						
Domain length (m)	100					
Spatial discretization	512					
Nonlinear order	5					
Duration of simulation (s)	300					
Temporal discretization (s)	0.1					

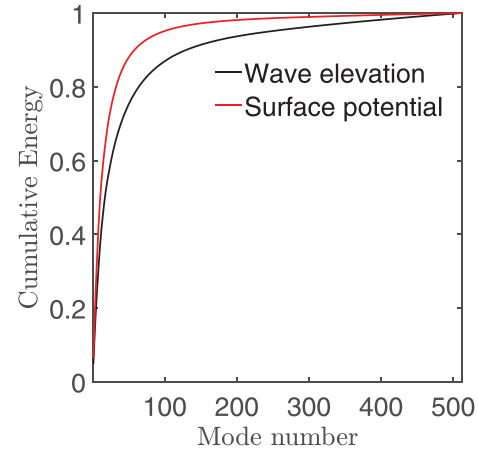


FIG. 8. Cumulative energy of POD modes of wave elevation and surface potential for general database of unidirectional irregular waves.

since the order of the modes ($r = 200$) is quite high, whereas for a single nonlinear regular wave case, $r = 6$. There is no significant advantage of having ROM2 for the case of unidirectional irregular waves. Both HOS and HOS-simple are faster than real-time and the HOS-simple model is around two orders of magnitude faster.

The total error metric, E_p , at a time step t over a range of n_s test samples is calculated as follows:

$$\mathcal{E}(t, i) = \left\| \frac{\eta^{t,i} - \hat{\eta}^{t,i}}{H_s} \right\|_2 / \sqrt{n_x}, \quad (20)$$

$$E(t) = \sum_{i=1}^{n_s} \mathcal{E}(t, i) / n_s.$$

Figure 10(a) depicts the propagation of total error, E_p , across all test samples, n_s , for each sea-state steepness. Without any intervention,

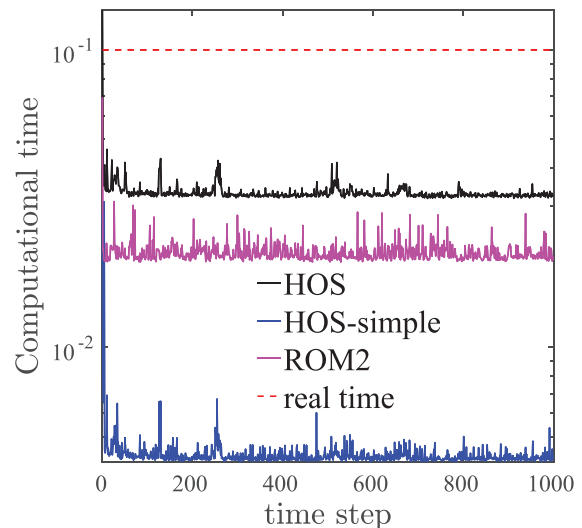


FIG. 9. Comparison of computational time per time step for unidirectional irregular wave.

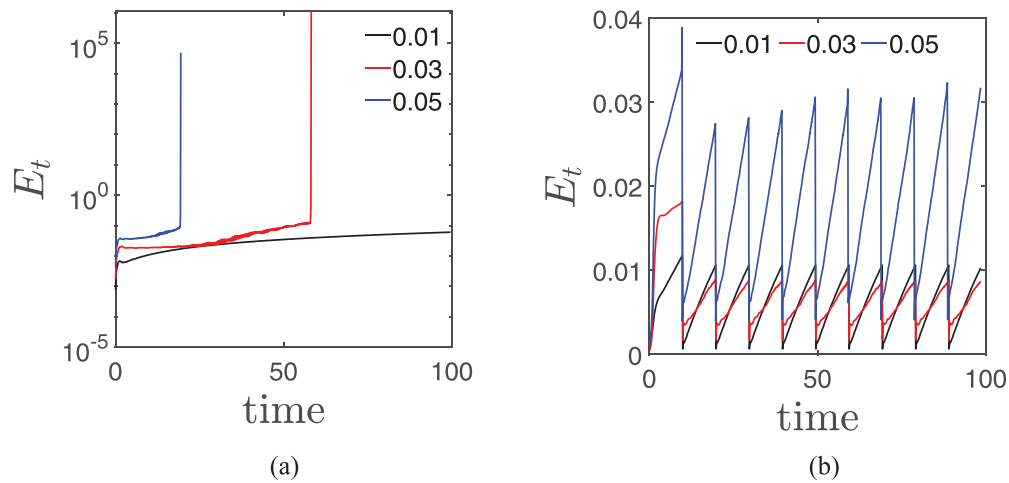


FIG. 10. Error propagation of HOS-simple across all samples of dataset (a) without intervention and (b) with intervention.

the error, E_t , increases with time and blows up after several time steps. It is not the case for all wave conditions but the behavior is computed after averaging over all cases. To mitigate this problem, we intervene in the time integration by providing the original solution of η and an estimate of τ_s from linear wave theory at every 100 time steps, effectively performing data assimilation at a fixed interval and re-compute the nonlinear wave evolution. This intervention reduces the error drastically as seen in Fig. 10(b). A sample plot of comparison between the HOS and HOS-simple models is provided in Fig. 11.

B. Multi-directional irregular waves

For the case of multi-directional irregular waves, a general database is generated using the parameters shown in Table V. In this case,

the spreading to generate multi-directional waves is provided to be $\pm 45^\circ$ and the mean direction is 0° . Also, around 100 cases are considered for each steepness; therefore, in total 600 simulations are carried out using HOS-Ocean to generate the synthetic database.

The operators of the reduced order model are computed from around 300 cases of training data and the prediction is carried out on completely unseen test cases with different steepness values and different wave conditions. Each wave simulation case has 3000 snapshots; however, we only consider every 15th snapshot for basis generation to reduce the data to be handled and also to consider sufficient distinction between adjacent snapshots.

Figure 12 depicts the cumulative energy captured by the POD modes in the system. Around 500 POD modes and 700 DEIM control points are used to construct the reduced order operators in the offline

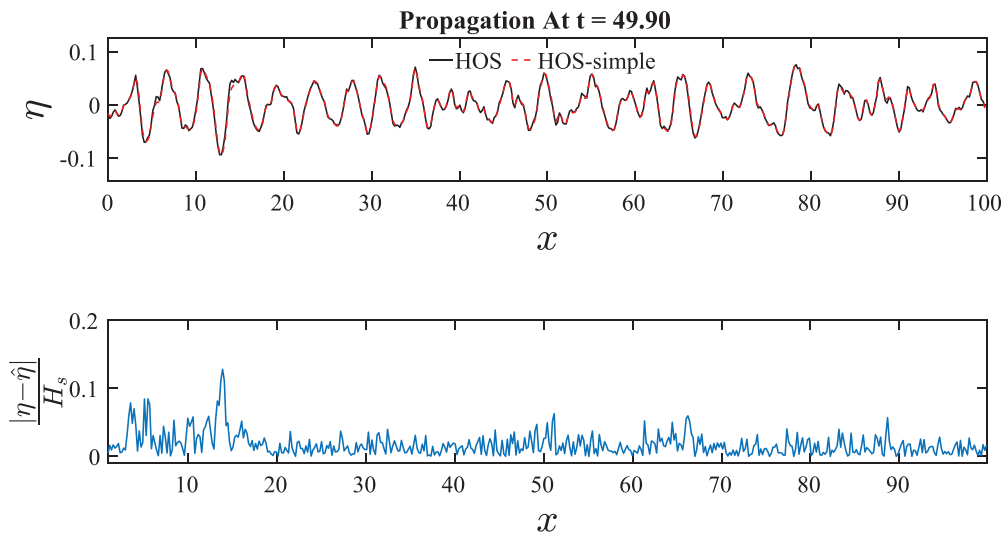


FIG. 11. Comparison between the HOS and HOS-simple models for unidirectional irregular wave with $H_s = 0.1296$ m and $T_p = 1.61$ s.

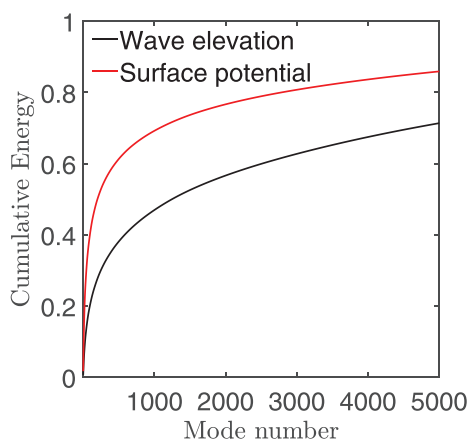
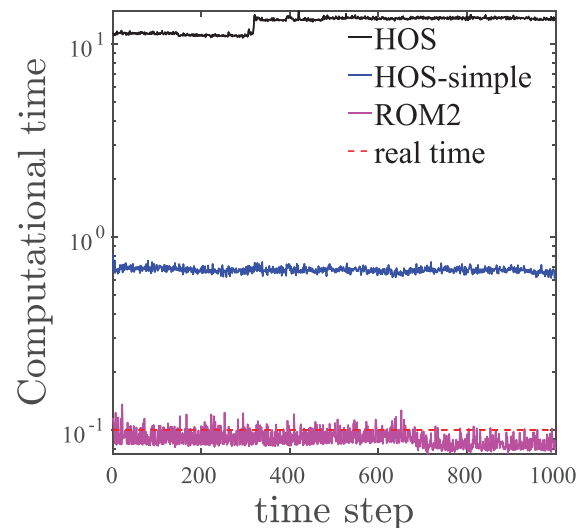
TABLE V. Parameters used to generate synthetic database of multi-directional irregular waves.

	Train			Test		
Sea-state steepness (H_s/T_p^2)	0.02	0.04	0.06	0.01	0.03	0.05
T_p (s)	1.0–4.0					
H_s (m)	Steepness* T_p^2					
Cases	100 Each					
Common simulation parameters						
Domain length in x (m)	60					
Domain length in y (m)	48					
Spatial discretization in x	256					
Spatial discretization in y	256					
Nonlinear order	5					
Duration of simulation (s)	300					
Temporal discretization (s)	0.1					

computation phase. ROM2 is also integrated in time with the same time step $dt = 0.1$ s to generate the results.

Figure 13 depicts the computational time required by HOS, HOS-simple, and ROM2 for a single case for qualitative comparison. The HOS and HOS-simple models are slower than real-time in the case of multi-directional waves. ROM2 with $r = 500$ is almost close to real-time but significantly faster than the HOS and HOS-simple models. Unlike unidirectional irregular waves, ROM2 shows greater speed up for multi-directional waves. From unidirectional to multi-directional waves, the order of ROM2 considered increases from $r = 200$ to $r = 500$ whereas for the full order models HOS and HOS-simple, the order of the problem increases from $N = 512$ to $N = 256 \times 256$. This significant increase on the order of the problem has led to tremendous increase in the computational time as evident from Figs. 13 and 9.

The same error metric, E_b , is computed for the randomly chosen test case for each steepness and is depicted in Fig. 14. Without any intervention of the original solution, the error, E_b , shoots up at


FIG. 12. Cumulative energy of POD modes of wave elevation and surface potential for general database of multi-directional irregular waves.

FIG. 13. Comparison of computational time per time step for multi-directional irregular waves.

different time instants for different wave steepness values. This blowup is avoided altogether by intervening in the time integration with the original solution every 100 time steps. The error, E_b , is significantly reduced and the computation becomes stable with this intervention as seen from Fig. 14(b).

A sample plot of comparison between HOS and ROM2 is provided in Fig. 15. It can be seen that ROM2 is able to reproduce the short-crested wave-field relative to HOS taken as reference wave-field with reasonably good agreement. The comparisons for both long-crested and short-crested waves demonstrate the applicability and performance of the proposed ROM.

V. POTENTIAL REAL-WORLD APPLICATIONS

In this section, we discuss the potential use of the proposed ROM for real-world applications. The applications of ROM and the parameters used to build ROM are summarized in Fig. 16.

A. Wave-field prediction based on upstream wave probe

One potential application of ROM is to enhance the predictability of phase-resolved wave-fields in a wave tank or ocean basin based on upstream wave probe(s). Such a capability could be fed into the real-time control algorithm of the following examples that can be tested in a controlled environment: vessels with dynamic positioning (DP), turret-moored vessel with heading control ability, renewable marine energy device in response actively to incoming wave-field, or navigation of remotely controlled and autonomous vessels.

Here, we provide an example using physical experiment conducted in TCOMS ocean basin to validate the performance of ROMs. A schematic diagram of the basin and the experimental setup is shown in Fig. 17. The dimension of the basin is 60 m in length \times 48 m in breadth, with water depth set at 10 m. The basin is equipped with wave paddles along the west and southern sides for wave generation, and beaches along the northern and eastern sides for wave absorption.

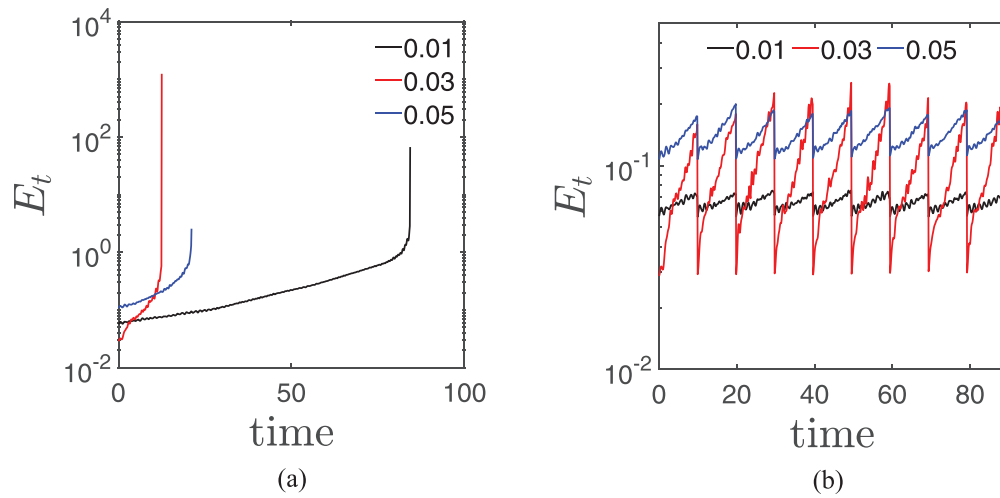


FIG. 14. Error propagation of ROM2 for multi-directional irregular waves (a) without intervention and (b) with intervention.

The beach along the northern side can be retracted to form a wall if needed.

In this experiment, we generated long-crested irregular waves along the $+x$ direction in the basin. The north side beach was folded up as a wall to prevent wave dissipation along the north side. Four

wave probes were installed along the centerline ($y = 24$ m), at $x = 8.40, 9.34, 9.84$, and 30.00 m. As the wave propagates along the $+x$ direction. Probes 1, 2, and 3 are referred to as upstream probes, while probe 4 is referred to as downstream probe. All probes measured at a sampling rate of 128 Hz.

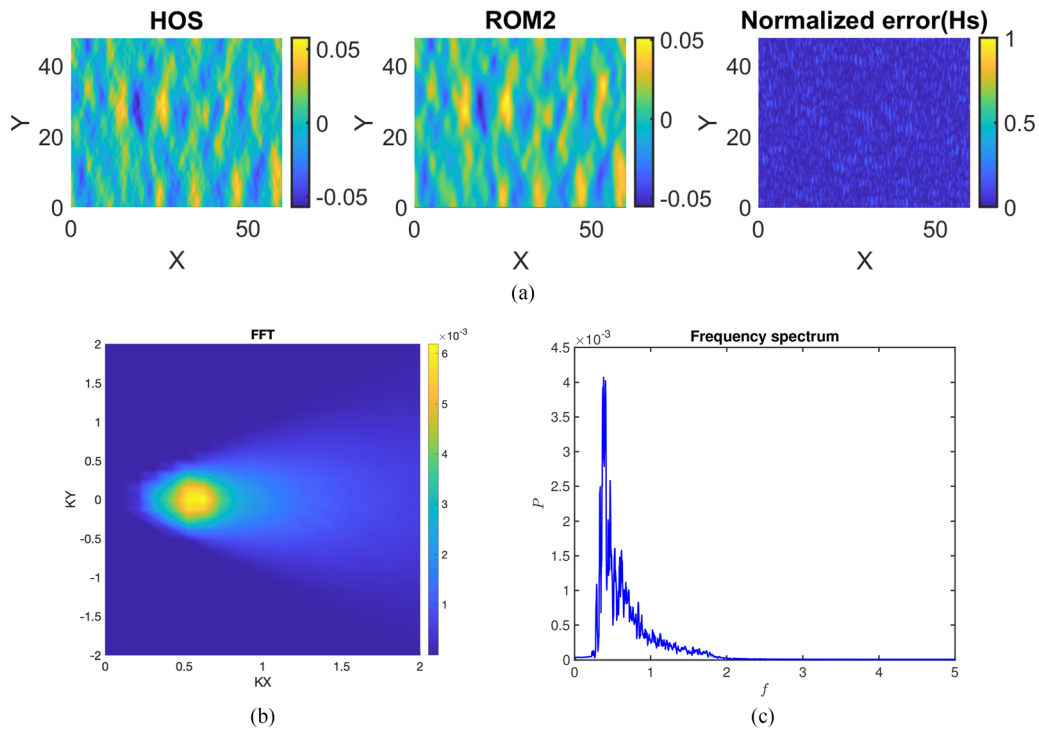


FIG. 15. (a) Comparison between the standard HOS model and ROM2 for multi-directional irregular waves with $H_s = 0.0681$ m and $T_p = 2.6090$ s. (b) Wavenumber spectrum and (c) frequency spectrum of the above case.

Parameters to build ROM for
Uni-directional irregular waves

Table IV

ROM

Application of ROM for Wave propagation
From upstream to downstream in a wave tank

Figure 17

Parameters to build ROM for
Multi-directional irregular waves

Table V

ROM

Application of ROM for Wave propagation
From far field to near field in a open ocean

Figure 19

FIG. 16. Summary of applications of ROM in the current work.

The procedure for the validation of ROM is as follows:

1. collect surface elevation-time histories, $\eta^{up}(t)$, $t \in [t_0 - \tau, t_0]$ of the upstream probes for τ seconds;
2. estimate the wave amplitudes, A_i , and phases, ϕ_i , from the time histories by least square fitting their Fourier components;
3. construct the initial wave-field, $\eta^{init}(x, t_0)$, based on the components estimated, i.e., $\eta^{init}(x, t_0) = \sum_i A_i \cos(\omega_i t_0 - k_i x + \phi_i)$;
4. estimate the initial surface velocity potential, Ψ^{init} , from $\eta^{init}(x, t_0)$ using linear wave theory; and
5. propagate the initialized wave-field using HOS and in particular ROM2 in space and time, and then validate their results with the downstream probe measurement.

We validate our numerical model with long-crested irregular waves based on JONSWAP spectrum with $H_s = 0.15$ m, $T_p = 2.02$ s, and $\gamma = 3.3$. The time interval is chosen to be $[50 - 10T_p, 50]$ to avoid the starting transient and the reflection built up from the beach. Based on the time interval chosen and the location of the upstream probes, one can compute the predictable time interval at the downstream probe. The detailed derivation of the predictable zone is discussed in

Ref. 38 and is not shown here for brevity. A comparison of the numerical model with the experimental result is shown in Fig. 18. The error, \mathcal{E} , is computed using the time history within the predictable zone based on Eq. (20), and it is found that both HOS and ROM2 have comparable errors, which are 5.8% and 5.5%, respectively. This implies that while ROM2 is simplified by the assumption in Eq. (17), it is sufficiently accurate in regard to wave-field propagation.

B. Wave-field prediction based on X-band radar

Nowadays, X-band radars measuring phase-resolved wave information on-board of a ship or a floating platform have become increasingly common, see, e.g., FutureWaves (<https://www.futurewavesradar.com/>) and WaMoS (<https://rutter.ca/wamos/>). The advantage of such a capability is to enable the prediction of operating wave-fields that the ship/platform will encounter, which translates into a prediction of the ship/structure motion response confined within the prediction window or lead time. This capability has widespread applications in shipping and marine and offshore industries such as route planning, helicopter takeoff and landing, ship-to-ship operation or installation of wind turbine platform that requires lead time of the order of seconds to minutes.

Figure 19 illustrates two possible scenarios on the use of X-band radars. The first scenario is for a floating or a bottom-founded platform that is moored or fixed to the seabed. The X-band radar provides measurement coverage of wave-fields at the far-field, denoted by the black color box. The actual dimension of the coverage, resolution, and sampling rate depends on the individual radar. The objective is to predict ahead of time the resulting wave-field that would arrive at the location of the platform some time later. For steep sea-states, the nonlinear effects of wave-wave interactions become important and hence the use of nonlinear wave evolution models such as HOS will be required. Therefore, the proposed ROM is useful as the computational efficiency, in particular in handling multi-directional evolution of wave-fields, has been improved to real-time.

The second scenario is for a ship with forward speed (or moving vessel). Obviously, compared to the first scenario, the prediction horizon or the lead time for this scenario will be shorter because, prediction region in the near-field will also move together with ship's

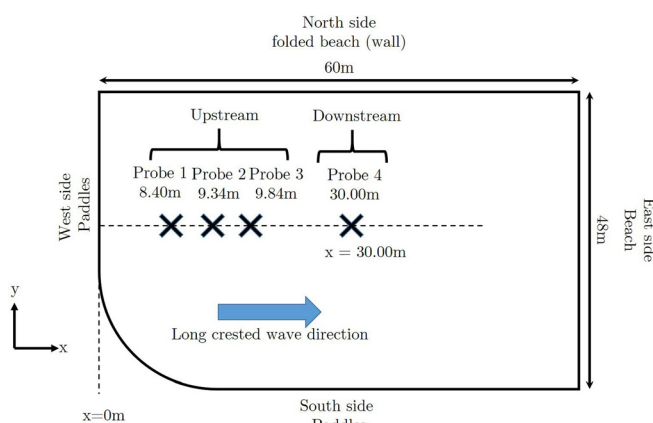


FIG. 17. Schematic diagram of the basin and the probe setup.

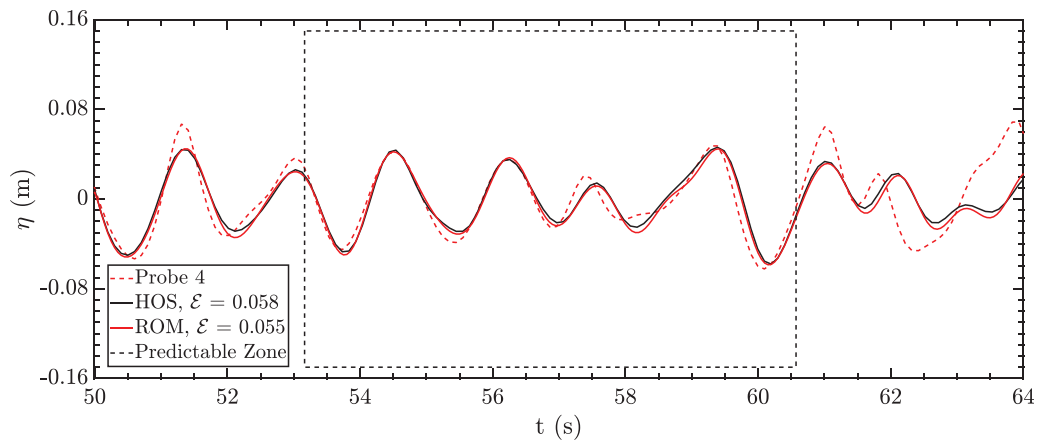


FIG. 18. Comparison of surface elevation-time histories between measurement from downstream probe (probe 4) and predictions from HOS and ROM2 for long-crested irregular waves with $H_s = 0.15$ m, $T_p = 2.02$ s, and $\gamma = 3.3$. The prediction error is lower within predictable zone ($t \in [53, 60.5]$ s), and it gets very high beyond the predictable zone.

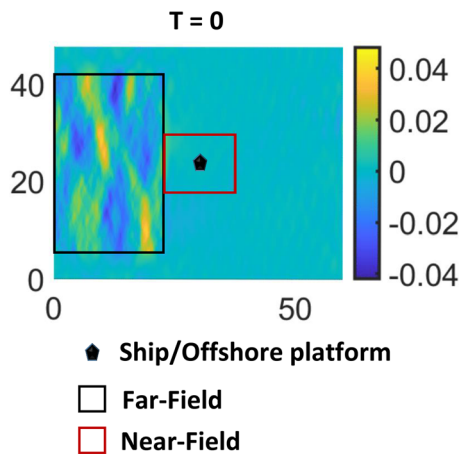


FIG. 19. An X-band radar on-board of a ship/platform measuring far-field multi-directional wave-fields.

forward motion, and this adds onto the requirement for fast and efficient wave prediction model. The proposed ROM approach, once extended to account for ships with forward speed, may be of significant value.

Figure 20 illustrates the comparison for the first scenario between the reference wave-field and the ROM predicted wave-field at the near-field 10 s later based upon initial measurements at the far-field. It can be seen that ROM will propagate the wave-field from far-field to near-field, and in this case reasonably good agreement can be observed. The predicted wave-field can be further fed into a hydrodynamic model to obtain the prediction of platform motion response and this will be investigated in the near future.

VI. CONCLUSIONS

In this work, we have developed a projection-based reduced order model (ROM) of the higher order spectral (HOS) method for the nonlinear evolution of ocean waves. A Galerkin projection of the Zakharov equations is carried out onto the dominant modes computed from proper orthogonal decomposition (POD). We also

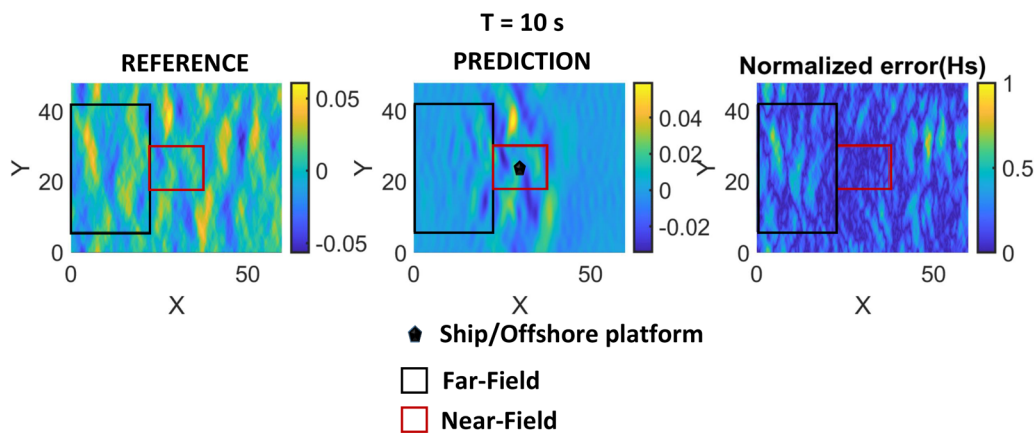


FIG. 20. Far-field to near-field wave propagation by ROM2 for a given far-field multi-directional wave measured by an X-band radar on-board of a moored offshore platform.

introduce an alternative formulation to compute the vertical water particle velocity underneath the free surface. This alternative formulation, referred to as HOS-simple in this work, paves the way for an efficient implementation of projection-based ROM. The ROM2 deduced from the Galerkin projection of HOS-simple is found to be computationally efficient. Further work will be undertaken to improve the difference in phase velocity of the underlying wave-fields observed in the ROM2 and HOS-simple models as compared to the standard HOS method. At present, the practical solution is to introduce intervention, interpreted as data assimilation at a fixed interval; by doing so, the prediction error can be contained within a reasonable range. For unidirectional irregular waves, ROM2 offers no substantial advantage because both the HOS and HOS-simple models are much faster than real-time. The true advantage is demonstrated in multi-directional irregular waves, where ROM2 is the only model capable of achieving real-time computation; hence, phase-resolved wave prediction in real-time becomes possible. We also demonstrate the potential use of ROM2 for real-world applications involving a wave tank or controlled environment and open ocean.

ACKNOWLEDGMENTS

This research is supported by A*STAR Science and Engineering Research Council, Singapore with Grant No. 172 19 00089 under the Marine & Offshore Strategic Research Programme (M&O SRP). The computational work for this article was partially performed on resources of the National Supercomputing Center, Singapore (<http://www.nscg.sg>).

AUTHOR DECLARATIONS

Conflict of Interest

The authors have no conflicts to disclose.

DATA AVAILABILITY

The data that support the findings of this study are available from the corresponding author upon reasonable request.

REFERENCES

- ¹P. Benner, S. Gugercin, and K. Willcox, "A survey of projection-based model reduction methods for parametric dynamical systems," *SIAM Rev.* **57**(4), 483–531 (2015).
- ²F. Bonnefoy, G. Ducroz, D. Le Touzé, and P. Ferrant, "Time domain simulation of nonlinear water waves using spectral methods," in *Advances in Numerical Simulation of Nonlinear Water Waves* (World Scientific, 2010), pp. 129–164.
- ³N. Booi, R. C. Ris, and L. H. Holthuijsen, "A third-generation wave model for coastal regions: 1. Model description and validation," *J. Geophys. Res.* **104**, 7649–7666, <https://doi.org/10.1029/98JC02622> (1999).
- ⁴S. L. Brunton and B. R. Noack, "Closed-loop turbulence control: Progress and challenges," *Appl. Mech. Rev.* **67**(5), 050801 (2015).
- ⁵S. L. Brunton, B. R. Noack, and P. Koumoutsakos, "Machine learning for fluid mechanics," *Annu. Rev. Fluid Mech.* **52**, 477–508 (2020).
- ⁶S. Chaturantabut and D. C. Sorensen, "Nonlinear model reduction via discrete empirical interpolation," *SIAM J. Sci. Comput.* **32**(5), 2737–2764 (2010).
- ⁷D. G. Dommermuth and D. K. Yue, "A high-order spectral method for the study of nonlinear gravity waves," *J. Fluid Mech.* **184**, 267–288 (1987).
- ⁸G. Ducroz, H. B. Bingham, A. P. Engsig-Karup, F. Bonnefoy, and P. Ferrant, "A comparative study of two fast nonlinear free-surface water wave models," *Int. J. Numer. Methods Fluids* **69**(11), 1818–1834 (2012).
- ⁹G. Ducroz, F. Bonnefoy, D. Le Touzé, and P. Ferrant, "HOS-ocean: Open-source solver for nonlinear waves in open ocean based on high-order spectral method," *Comput. Phys. Commun.* **203**, 245–254 (2016).
- ¹⁰G. Ducroz, F. Bonnefoy, D. L. Touzé, and P. Ferrant, "3-D HOS simulations of extreme waves in open seas," *Nat. Hazards Earth Syst. Sci.* **7**(1), 109–122 (2007).
- ¹¹H. Eivazi, H. Veisi, M. H. Naderi, and V. Esfahanian, "Deep neural networks for nonlinear model order reduction of unsteady flows," *Phys. Fluids* **32**(10), 105104 (2020).
- ¹²F. Fang, C. Pain, I. Navon, M. Piggott, G. Gorman, P. Allison, and A. Goddard, "Reduced-order modelling of an adaptive mesh ocean model," *Int. J. Numer. Methods Fluids* **59**(8), 827–851 (2009).
- ¹³J. D. Fenton, "Numerical methods for nonlinear waves," in *Advances in Coastal and Ocean Engineering* (World Scientific, 1999), pp. 241–324.
- ¹⁴L. Fernandez, M. Onorato, J. Monbaliu, and A. Toffoli, "Modulational instability and wave amplification in finite water depth," *Nat. Hazards Earth Syst. Sci.* **14**(3), 705–711 (2014).
- ¹⁵K. Fukunaga, *Introduction to Statistical Pattern Recognition* (Elsevier, 2013).
- ¹⁶I. Gatin, V. Vukčević, and H. Jasak, "A framework for efficient irregular wave simulations using higher order spectral method coupled with viscous two phase model," *J. Ocean Eng. Sci.* **2**(4), 253–267 (2017).
- ¹⁷T. W. Group, "The WAM model: A third generation ocean wave prediction model," *J. Phys. Oceanogr.* **18**(12), 1775–1810 (1988).
- ¹⁸T. Hlophe, H. Wolgamot, A. Kurniawan, P. H. Taylor, J. Orszaghova, and S. Draper, "Fast wave-by-wave prediction of weakly nonlinear unidirectional wave fields," *Appl. Ocean Res.* **112**, 102695 (2021).
- ¹⁹P. Holmes, J. L. Lumley, G. Berkooz, and C. W. Rowley, *Turbulence, Coherent Structures, Dynamical Systems and Symmetry* (Cambridge University Press, 2012).
- ²⁰K. Karhunen, "Zur spektraltheorie stochastischer prozesse," *Ann. Acad. Sci. Fenn.* **34**, 1–7 (1946).
- ²¹M. Kirby and L. Sirovich, "Application of the Karhunen-Loeve procedure for the characterization of human faces," *IEEE Trans. Pattern Anal. Mach. Intell.* **12**(1), 103–108 (1990).
- ²²N. Köllisch, J. Behrendt, M. Klein, and N. Hoffmann, "Nonlinear real time prediction of ocean surface waves," *Ocean Eng.* **157**, 387–400 (2018).
- ²³D. D. Kosambi, "Statistics in function space," *J. Indian Math. Soc.* **7**, 76–88 (1943).
- ²⁴M. Loeve, "Sur les fonctions aleatoires stationnaires du second ordre," *Rev. Sci.* **83**, 297–303 (1945).
- ²⁵Z. Luo, J. Zhu, R. Wang, and I. M. Navon, "Proper orthogonal decomposition approach and error estimation of mixed finite element methods for the tropical Pacific Ocean reduced gravity model," *Comput. Methods Appl. Mech. Eng.* **196**(41–44), 4184–4195 (2007).
- ²⁶R. Maulik, B. Lusch, and P. Balaprakash, "Reduced-order modeling of advection-dominated systems with recurrent neural networks and convolutional autoencoders," *Phys. Fluids* **33**(3), 037106 (2021).
- ²⁷S. Pawar, S. Rahman, H. Vaddireddy, O. San, A. Rasheed, and P. Vedula, "A deep learning enabler for nonintrusive reduced order modeling of fluid flows," *Phys. Fluids* **31**(8), 085101 (2019).
- ²⁸Y. Qi, G. Wu, Y. Liu, M.-H. Kim, and D. K. Yue, "Nonlinear phase-resolved reconstruction of irregular water waves," *J. Fluid Mech.* **838**, 544 (2018).
- ²⁹C. W. Rowley and S. T. Dawson, "Model reduction for flow analysis and control," *Annu. Rev. Fluid Mech.* **49**, 387–417 (2017).
- ³⁰A. Sergeeva and A. Slunyaev, "Rogue waves, rogue events and extreme wave kinematics in spatio-temporal fields of simulated sea states," *Nat. Hazards Earth Syst. Sci.* **13**(7), 1759–1771 (2013).
- ³¹K. Taira, S. L. Brunton, S. T. Dawson, C. W. Rowley, T. Colonius, B. J. McKeon, O. T. Schmidt, S. Gorddeyev, V. Theofilis, and L. S. Ukeiley, "Modal analysis of fluid flows: An overview," *AIAA J.* **55**(12), 4013–4041 (2017).
- ³²M. Tanaka, "Verification of Hasselmann's energy transfer among surface gravity waves by direct numerical simulations of primitive equations," *J. Fluid Mech.* **444**, 199–221 (2001).
- ³³A. Toffoli, O. Gramstad, K. Trulsen, J. Monbaliu, E. Bitner-Gregersen, and M. Onorato, "Evolution of weakly nonlinear random directional waves: Laboratory experiments and numerical simulations," *J. Fluid Mech.* **664**, 313–336 (2010).

- ³⁴A. Toffoli, M. Onorato, E. Bitner-Gregersen, and J. Monbaliu, "Development of a bimodal structure in ocean wave spectra," *J. Geophys. Res.* **115**(C3), 005495, <https://doi.org/10.1029/2009JC005495> (2010).
- ³⁵H. L. Tolman *et al.*, "User manual and system documentation of WAVEWATCH III TM version 3.14. Technical note," *MMAB Contrib.* **276**, 220 (2009).
- ³⁶B. J. West, K. A. Brueckner, R. S. Janda, D. M. Milder, and R. L. Milton, "A new numerical method for surface hydrodynamics," *J. Geophys. Res.* **92**(C11), 11803–11824, <https://doi.org/10.1029/JC092iC11p11803> (1987).
- ³⁷A. P. Wijaya, P. Naaijen, E. van Groesen *et al.*, "Reconstruction and future prediction of the sea surface from radar observations," *Ocean Eng.* **106**, 261–270 (2015).
- ³⁸G. Wu, "Direct simulation and deterministic prediction of large-scale nonlinear ocean wave-field," Ph.D. thesis (Massachusetts Institute of Technology, 2004).
- ³⁹G. Wu, Y. Liang, W. Lin, H. Lee, and S. Lim, "A note on equivalence of proper orthogonal decomposition methods," *J. Sound Vib.* **265**, 1103–1110 (2003).
- ⁴⁰W. Xiao, Y. Liu, G. Wu, and D. K. Yue, "Rogue wave occurrence and dynamics by direct simulations of nonlinear wave-field evolution," *J. Fluid Mech.* **720**, 357–392 (2013).